Int. J. Electrochem. Sci., 8 **(2013)** 10586 - 10600

International Journal of ELECTROCHEMICAL SCIENCE
www.electrochemsci.org

Electrochemical Study of Sb-Doped SnO_2 Supports on the Oxygen Evolution Reaction: Effect of Synthesis Annealing Time

V. Ávila-Vázquez[1], *J.C. Cruz*[2], *M. Galván-Valencia*[1], *J. Ledesma-García*[3], *L.G. Arriaga*[4], *C. Guzmán*[1], *S. M. Durón-Torres*[1*]

[1] Unidad Académica de Ciencias Químicas–UAZ, CU Siglo XXI Edificio 6, Km 6 Carr. Zac – Gdl, La Escondida Zacatecas, C.P. 96160,
Zacatecas, México
[2] División de Estudios de Posgrado e Investigación, Instituto Tecnológico de Chetumal, Av. Insurgentes No. 330, C.P. 77013,Col. David Gustavo Gtz., Chetumal, Quintana Roo, México.
[3] División de Investigación y Posgrado, Facultad de Ingeniería, Universidad Autónoma de Querétaro, Cerro de las Campanas, C.P. 76010, Querétaro, México.
[4] Centro de Investigación y Desarrollo Tecnológico en Electroquímica S.C., Parque Tecnológico Querétaro, Sanfandila, 76703 Pedro Escobedo, Querétaro, México.
[*]E-mail: duronsm@prodigy.net.mx

Received: 18 May 2013 / *Accepted:* 3 July 2013 / *Published:* 1 August 2013

It has been recognized the role of supports in electrocatalysis as a way to increase both specific activity and lifetime of electrocatalysts. Due its stability, some doped SnO_2 supports could be used as an alternative to carbon black in PEM water electrolysis. In this work, IrO_2 catalyst was mixed in a colloidal mini-mill with SnO_2 supports doped with antimonium (ATO) in a fixed proportion (50:50 wt %) and the mixtures were used as anodic material for Oxygen Evolution Reaction (OER). ATO supports were obtained by reaction between Sn and Sb chloride precursors in alcoholic medium at moderate temperature, followed by an annealing procedure at 500 °C and different times of treatment (between 3 h and 15 h). The electrodes were evaluated in terms of OER by Linear Scan Voltammetry (LSV) and Electrochemical Impedance Spectroscopy (EIS) techniques. Electrokinetic parameters as Tafel Slope and Exchange Current Density for OER were obtained as a function of the different annealing times material support. Furthermore, the Charge Transfer Resistances (Rct) for oxygen evolution obtained from the Nyquist impedance spectra were compared. Although the LSV results showed a similar behavior for the OER of the several electrodes studied, the EIS analysis presented some distinctive Rct values for the electrodes assayed. The electrodes that showed minimum Rct values corresponded to those prepared with supports of 3 h of annealing time. These results could suggest that the ATO conductive properties depend on the time of thermal treatment of the oxide in the synthesis procedure.

Keywords: Antimonium doped tin oxide, Iridium Oxide, Oxygen evolution reaction, Unitized regenerative fuel cells.

1. INTRODUCTION

In recent years, new technologies are being developed for energy generation in a clean, efficient and sustainable way. The fuel cells (FC), water electrolyzers (WE) and the unitized regenerative fuel cells (URFC) that combines FC and WE in a single unit, represent viable options for electrochemical hydrogen production and power generation in an environmental friendly way. Although some of these devices are now commercially available, problems about the cost, availability and performance of catalysts and supports remain as the principal drawbacks of the hydrogen electrochemical energy conversion systems.

The electrochemical reactions of oxygen: oxygen reduction reaction (ORR) and the oxygen evolution reaction (OER) usually are the slowest reactions in FC, WE and URFC, and therefore the limiting factors for these devices developing. In this sense, an important number of studies are currently dedicated to promote the electrochemical reactions of fuel cells and electrolyzers mainly based on the research and developing of new effective electrode and support materials for oxygen reactions [1-9].

Although it is commonly acknowledged the use of noble metals as catalysts in FC and WE, it has been found that Pt and other electrocatalytic metals show a better performance in the ORR than in the OER, presenting a high overpotential for the oxygen evolution. It has been noted that the oxides of Ir and Ru, and their combination with other metals; produce materials that are more convenient for OER catalysts. By the other side, despite of that the Vulcan coal and others carbonaceous materials show a well behavior as catalytic supports in FC, the high electrical potential used in an electrolyzer corrodes them, producing degradation of carbon material and a loss of electrical contact. Consequently, the research studies in electrochemical devices besides of finding catalysts with an activity enough for both oxygen reactions are focused in obtain support materials with the sufficient stability and electronic conductivity required in the anodic conditions of a WE [10, 11].

In the FC a potential near of 1 V vs. ENH is reached at the operation conditions, while in the WE is necessary to apply a potential higher than 1.6 V vs. ENH for splitting the water into H_2 and O_2. An oxygen electrode in a URFC operates alternatively at these two potential values, so that it is not advisable to use Vulcan carbon as support for the preparation of electrodes. The main disadvantage is that the operation with high potentials promotes the degradation of coal, limiting the electron transfer when a URFC operates mainly in the fuel cell mode. For this reason it is necessary to find an alternative support, which must be stable to a high potential of operation and it provides a good electrical conductivity for the reactions of the oxygen electrode [12, 13].

Tin oxides have been used as transparent conductive films in liquid crystal displays, photodetectors, solar cells, gas sensors and protective films [14-17]. Recent studies have shown that the doped ceramic materials with a conductive material, as is the case of ATO, means a new field in the study of the electrode supports science [18-20]. The ATO has characteristics of high resistance to corrosion in acid media and when it is doped with conductive species as Sb^{5+}, its electrical conductivity increases to 10^2 or 10^3 Ω^{-1} cm^{-1}. Studies indicate that the ATO could be used as catalyst support for OER in WE, being reported an improvement in the stability of the support as compared with an undoped oxide, in the conditions of oxygen evolution [18,21]. Recent researches indicate that

the characteristics of micro-structural and the nano-metric size of the ATO both depend strongly on the heat treatment of oxide in the stages of synthesis and the relative amount of doping agent [19].

This paper shows the preliminary results of the study of the OER kinetics of an IrO_2 catalyst supported on synthesized ATO obtained at different times of heat treatment (between 3 h and 15 h). Over the different supports obtained were evaluated the dispersibility of catalyst and the OER kinetic parameters as Tafel slope and transfer charge resistance in acid medium. The study was based on cyclic voltammetry (CV), linear voltammetry (LV) and electrochemical impedance spectroscopy (EIS), electrochemical techniques.

2. EXPERIMENTAL

2.1 Synthesis of IrO_2 and antimony doped tin oxide (ATO)

The IrO_2 catalyst for OER was synthesized using a colloidal system that consist of mixing a 0.01M $H_2IrCl_6 \cdot nH_2O$ solution with 1M NaOH for 50 min at a temperature near to 100 °C. The dark iridium hydroxide precursor obtained was then annealed at 400°C for 1 h. The physicochemical characterization reported elsewhere indicates that IrO_2 thus obtained has a particle size in the 7-9 nm range and a BET surface area of 100 $m^2 g^{-1}$ [22,23].

ATO supports were obtained by reaction between $SnCl_4.5H_2O$ and $SbCl_3$ (StremChem) precursors in hydrochloric acid and alcoholic medium at moderate temperature (60 °C) for 4 h, followed by an annealing procedure at 500 °C and heat treatment times of 3 h, 6 h, 9 h and 15 h. In this work, the supports prepared by this procedure are denoted as ATO (# h) where # denotes the number of hours of thermal treatment.

2.2 Physicochemical characterization

The synthesized ATO powders were first analyzed by X-ray diffraction measurements, performed on a DMAX 2100 Rigaku Diffractometer using CuKα monochromatic radiation at 40 kV and 40 mA and 0.08° min^{-1}. In order to verify the presence of Sb in the SnO_2 a X - Ray fluorescence (XRF) analysis was performed on XRF Bruker AXS S4 Explorer Spectrometer, equipped with Rn-X ray source LiF 220 crystal analyzer and operated at a power of 1 kW with a 0.12° divergence collimate.

The nitrogen adsorption-desorption isotherms were recorded using an Autosorb iQ2 equipment. The specific surface area and the pore size distribution (average pore diameter and mean pore volume) were calculated by applying the BET equation to the nitrogen adsorption isotherm and the Barret-Joyner-Halender (BJH) method to the desorption branch of the nitrogen isotherm, respectively [24].

2.3 Electrochemical characterization

2.3.1 Electrodes preparation

The electrodes were prepared from a catalytic ink comprising 90 μL of Nafion ® (5 wt. %, Aldrich), 540 μL of ethanol spectroscopic grade, 6 mg of IrO_2 and 6 mg of ATO. The ink was obtained

using a FRITSCH/PULVERISETTE 23 mini-mill for a period of 0.5 h in order to homogenize the mixture and promote dispersion of the ink. Later, the resulting suspensions were hold in an ultrasonic bath for 0.5 h in aim to gain additional dispersion of mixture. Subsequently, a volume of each ink was deposited on a clean polished glassy carbon disk electrode (GCE) (A = 0.07068 cm^2). The coated GCEs were dried in a furnace at 80°C for 10 min. In order to comparison a Pt supported on ATO (3h) electrode and an IrO_2 supported on Vulcan carbon electrode were used. Finally, IrO_2 and Pt films supported on ATOs were used as working electrodes for the OER kinetic studies. All the current values reported in this paper are normalized to the electrode geometric area.

2.3.2 Electrochemical characterization of electrodes

All the experiments were performed in a double-compartment electrochemical glass cell. An $Hg/Hg_2SO_4/0.5$ M H_2SO_4 (ESM = 0.69V vs. NHE) electrode was used as reference which was positioned as close to the working electrode as possible by means of a Luggin capillary. A Pt-mesh was used as counter-electrode and the aqueous electrolytic medium was 0.5 M H_2SO_4 at room temperature. The electrochemical measurements were performed using an EG&G PAR VersaSTAT 3 Potentiostat/Galvanostat. In this study, all measured values of potential are reported respect to the normal hydrogen electrode (NHE).

Cyclic voltammetry (CV) was carried out to evaluate the effect of different ATO in the IrO_2 or Pt electrodes by scanning the potential at a rate of 50 mV s^{-1} between -0.16 V and 1.54 V under a N_2 atmosphere electrolyte solution. Oxygen evolution experiments were performed by linear scan voltammetry (LSV) at a scan rate of 5 mV s^{-1} in the anodic direction from 0.59 V to 1.69 V in O_2-free electrolyte solution at a constant electrode rotation frequency of 1000 rpm. The rotation rate was controlled by a PINE MSRX precision rotating system.

In addition, electrochemical impedance spectroscopy (EIS) experiments were carried out in the potentiostatic mode in the 100 kHz to 10 mHz frequency range. The impedance spectra were registered with a logarithmic data collection scheme at 10 steps per decade at 1.57 V of potential with an alternate signal amplitude of 10 mV.

3. RESULTS

3.1 Physicochemical properties of ATO

The XRD diffraction patterns of ATO are shown in Fig. 1, here the characteristic peaks of SnO_2 with a cassiterite tetragonal structure and a rutile phase can be observed. Due to the minimal dopant quantity used, any diffraction peak related with Sb could be identified. After a Debye-Scherrer treatment of diffractograms the mean crystal size of the different ATO could be obtained. In Fig. 2 the particle size of ATO as a function of the calcination time is presented, the sizes obtained are in the 5.6 nm to 7.3 nm interval and as it was expected the crystal size increases as annealing time is rising.

The Sb presence in supports was verified by XRF and the results of elemental analysis are showed in Table 1, here can be observed that the antimony quantity in ATO slightly depends on the

annealing time with a maximum near of 9% in weight corresponding to a calcination time of 3 h. At 15 h of annealing time the Sb amount obtained was near of 7%, this decrease can be attributed to a selective material loss due the thermal treatment.

Table 1. XRF analysis of ATO annealed at 500°C.

Time of heat treatment / hr	Sn wt %	Sb wt %	Cl wt %
3	89.8	9.18	1.02
6	90.5	8.59	0.91
9	90.8	8.34	0.86
15	91.26	7.63	0.4

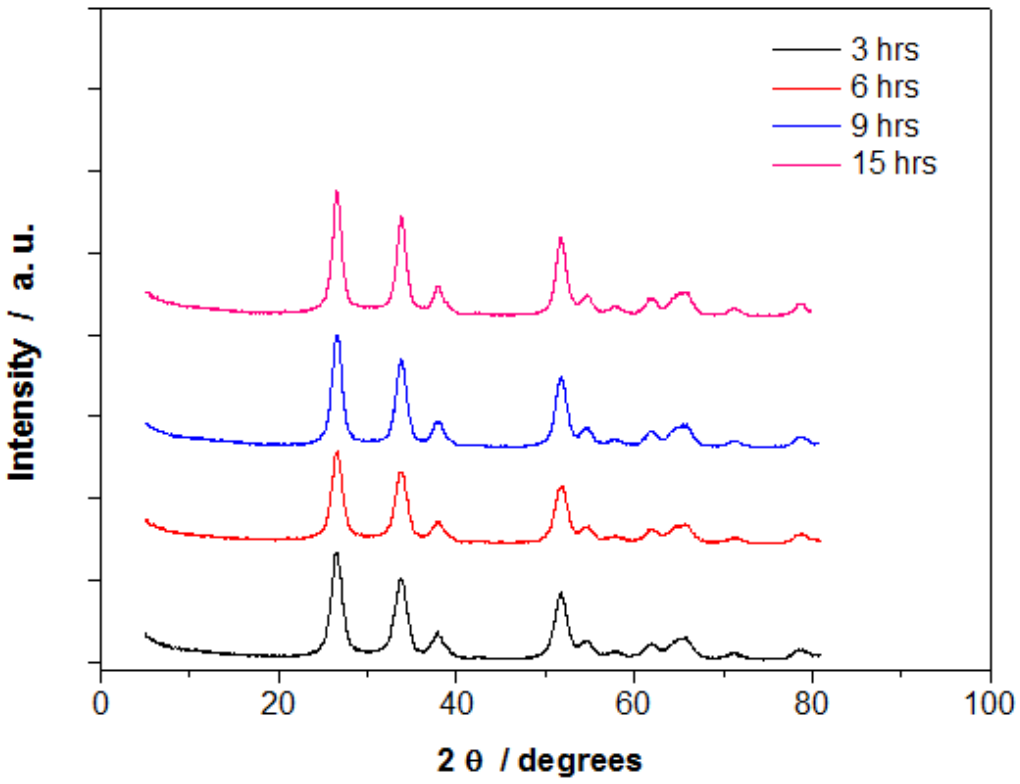

Figure 1. X-ray diffraction patterns of ATOs obtained at 500 °C and different heat treatment times.

For all annealing times the Sn amount was nearly constant to 90%. Also, in the XRF data it is possible to observe the presence of small quantities of chlorine as a residue of the precursor salts, the percentage of residual Cl is reduced when the annealing time increases.

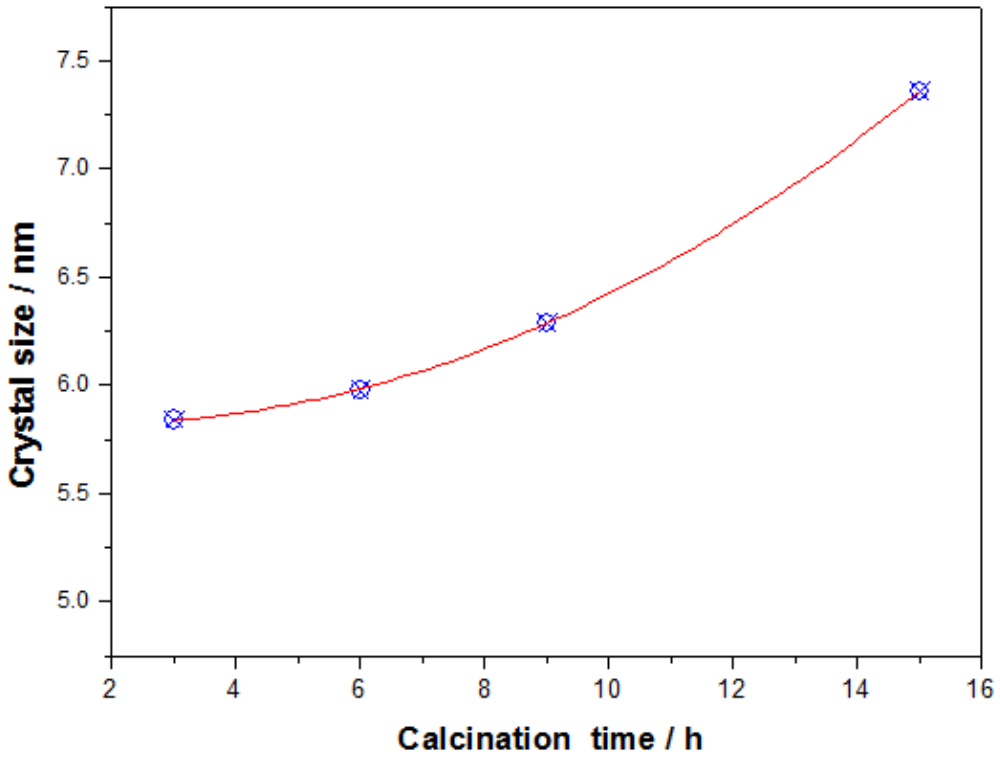

Figure 2. Crystal size of ATO obtained from X-ray diffraction as a calcination time function.

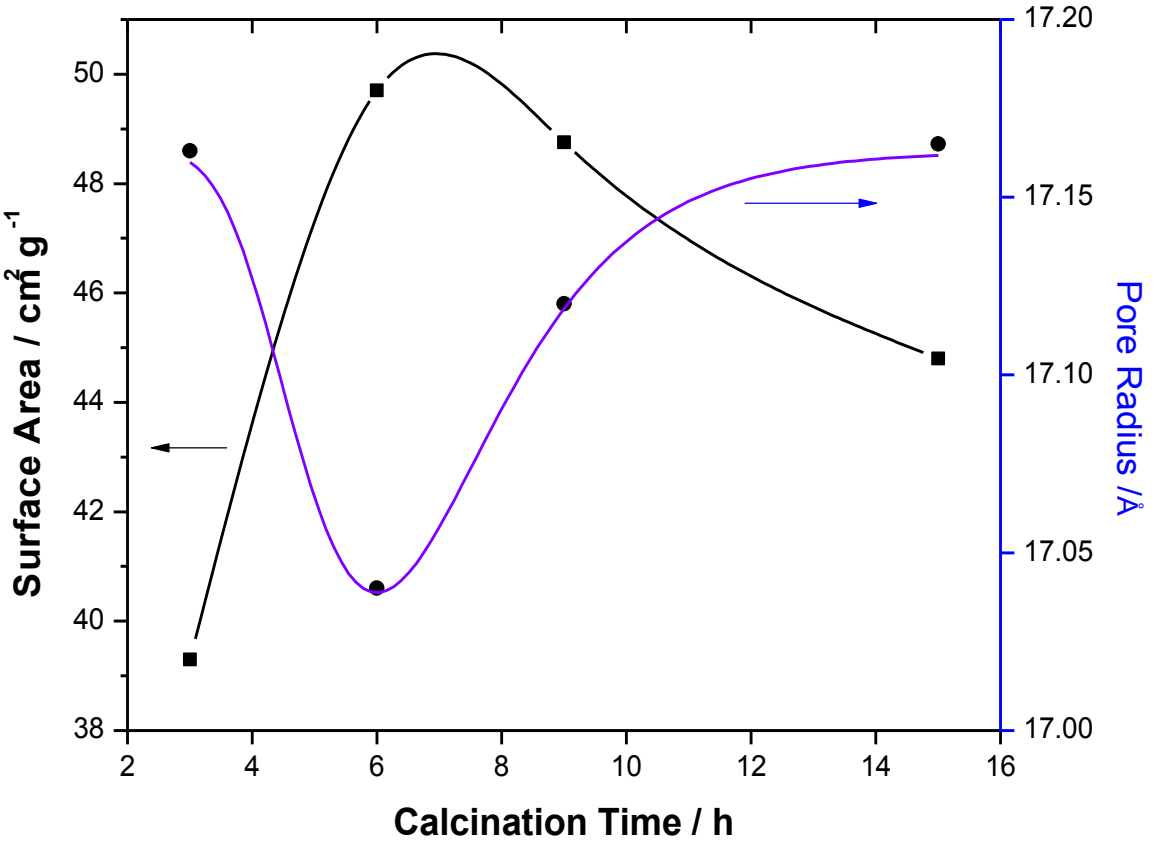

Figure 3. BET analysis of ATO obtained at 500 °C with different calcination times. The traced lines are a rough approximation to experimental trend.

Porosity and surface area of ATO were obtained by mean a BET analysis, in the Figure 3 are shown the interfacial properties of supports as a annealing time function. It is possible to observe that ATO calcinated at 500 °C during 6 h presented a surface area near to 50 m^2 g^{-1}, this area is higher approximately 10 m^2 g^{-1} than those obtained for ATO calcinated during 3 h. In correspondence the pore size in ATO(6h) is lightly smaller than found in ATO (3h). This behavior could be attributed to the thermal evolution of occluded water that generate more porosity at higher calcination times. For annealing times > 6h the surface area is decreased down to 45 m^2 g^{-1}due to a particle agglomeration process. The pore radius obtained in the supports was in all the cases near to 1.7 nm, thus all the ATO supports obtained in this work could be classified as mesoporous materials.

3.2 Evaluation of the supports by cyclic voltammetry

Figure 4 shows cyclic voltammograms obtained for IrO_2 supported on ATO in N_2 saturated 0.5 M H_2SO_4 solution. The CV diagrams reveal that the electrochemical response for IrO_2 is practically unchanged with the use of different ATO as support. Also is shown that the current density (j) attributed to IrO_2 supported on ATO (3h) and ATO (9h) are greater than the rest of the ATO's powders, this enhancement may be considered evidence that the dispersion of IrO_2 is improved with the use of this supports. The off-peak potential for oxygen evolution on all the IrO_2/ATO electrodes appears near to 1.45 V, although on the ATO(3h) and ATO(9h) supported electrodes the onset was about 50 mV more negative than the rest of ATOs as shown in Figure 4.

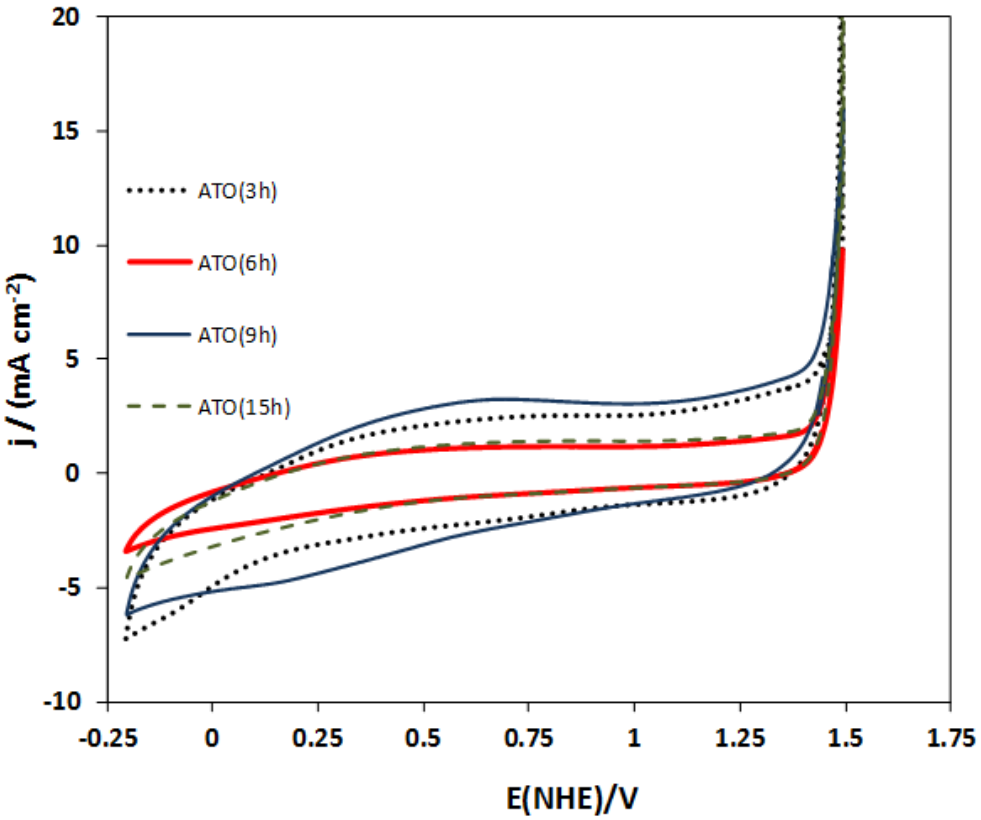

Figure 4. Cyclic voltammograms of GCEs coated with IrO_2/ATOs (with different heat treatment times: 3h, 6h, 9h and 15h) in 0.5 M H_2SO_4 at 50 mV s-1. 50 wt % IrO_2/ATOs, with atmosphere: N_2 and room temperature.

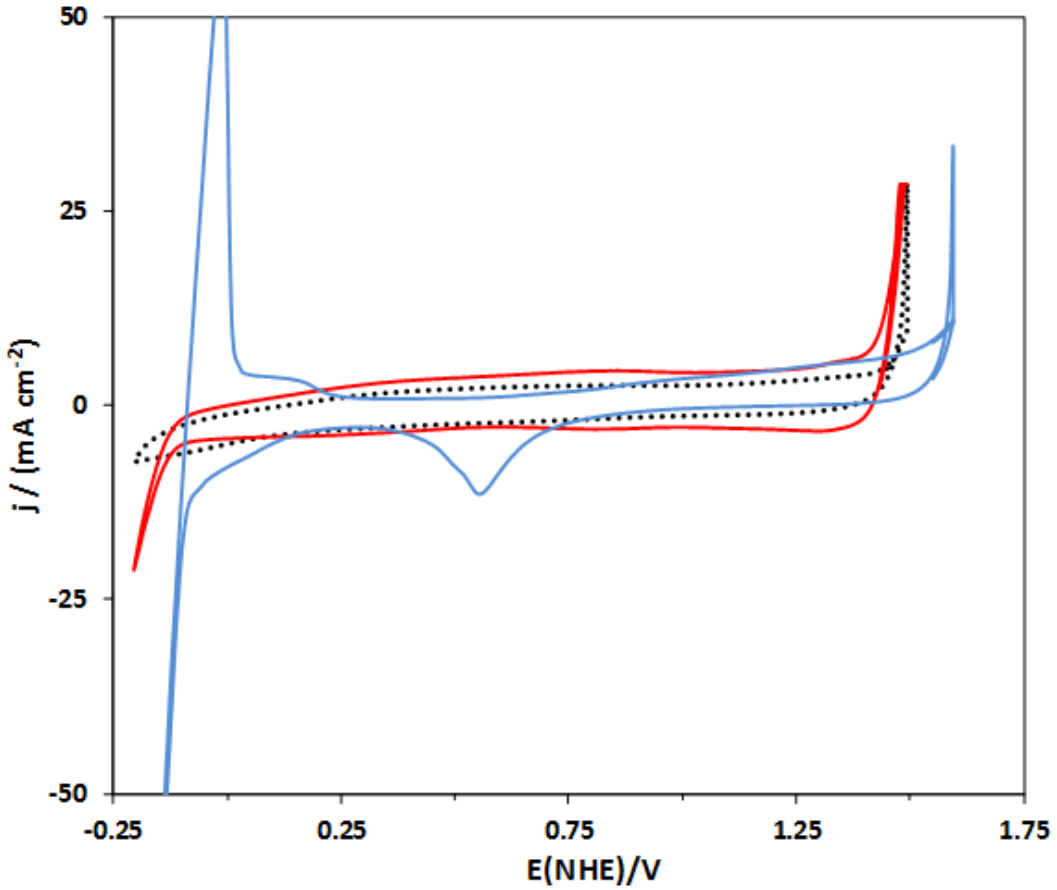

Figure 5. Cyclic voltammograms of IrO_2/ATO (3h) (black points), Pt/ ATO (3h) (blue line) and IrO_2/C (red line) electrodes in N_2 satured 0.5 M H_2SO_4 at 50 mV s^{-1}.

Figure 5 compares the cyclic voltammograms obtained for IrO_2 and Pt supported on ATO (3h) and IrO_2 supported on Vulcan carbon in N_2 saturated 0.5 M H_2SO_4 solution. The CV of Pt supported on ATO (3h) shows that the reactions associated with the surface of Pt in an acid medium are limited by the support, avoiding identify the characteristic peaks of Pt on a clearly way [25], nevertheless the general electrochemical behavior in acid medium of platinum is still outlined in the voltammogram. The voltammograms corresponding to IrO_2 catalyst show broad waves corresponding to the redox reactions over the Ir surface, these waves are more evident when Vulcan is used as support. In the voltammograms of Figure 5 also can be observed that the potential onset for oxygen evolution in the Pt/ATO electrode appears near to 1.7 V, while the corresponding oxygen evolution peaks of IrO_2/ATO and IrO_2/C electrodes appear about 300 mV more negative potential values.

3.3 Oxygen evolution activity of the IrO_2 supported on ATO

Figure 6 shows linear scan voltammograms for OER with IrO_2 support on ATO (with different heat treatment times: 3h, 6h, 9h and 15h) in 0.5 M H_2SO_4 at a scan rate of 5 mVs^{-1}. Since the IrO_2 catalyst used in the electrode preparation was the same in the different mixtures, and the proportion catalyst-support was maintained fixed in a 50:50 weight percent ratio, the voltammograms

displacement observed in Figure 6 indicate that the OER depend on the ATO annealing times used in the electrodes. It is observed that the OER begins in a potential near to 1.45 V when the IrO_2 is supported on ATO (3h), while for the IrO_2 supported on other ATO, EOR onset occurs near to 1.5 V. It means that EOR is favored when ATO 3h annealed is used as support for IrO_2. As a consequence, the higher current densities obtained when the ATO (3h) is used as a support for EOR. In Table 2, the values of current density obtained at a potential of 1.57 V along with other kinetic properties corresponding to the different IrO_2/ATO electrodes studied, are showed.

Table 2. Onset potential and kinetics parameters for OER on IrO_2/ATO electrodes in O_2 free 0.5 M H_2SO_4.

	E_{OER} (NHE)/V	j /(mA cm^{-2}) @ 1.57 V	Rs / Ω cm^2	Rct / Ω cm^2 @ 1.57 V	b / (mV dec^{-1}) η_{low}	η_{high}
IrO_2/ATO(3h)	1.5	16.2	0.28	2.97	62	-
IrO_2/ATO(6h)	1.55	5.7	0.21	16.26	68	-
IrO_2/ATO(9h)	1.55	4.5	0.25	22.69	78	120
IrO_2/ATO(15h)	1.55	4.5	0.32	40.78	75	122
IrO_2/C	1.41	-	0.29	20.07 @ (1.49V)	60	-
Pt/ATO(3h)	2	-	0.48	74.21 @ (2V)	-	-

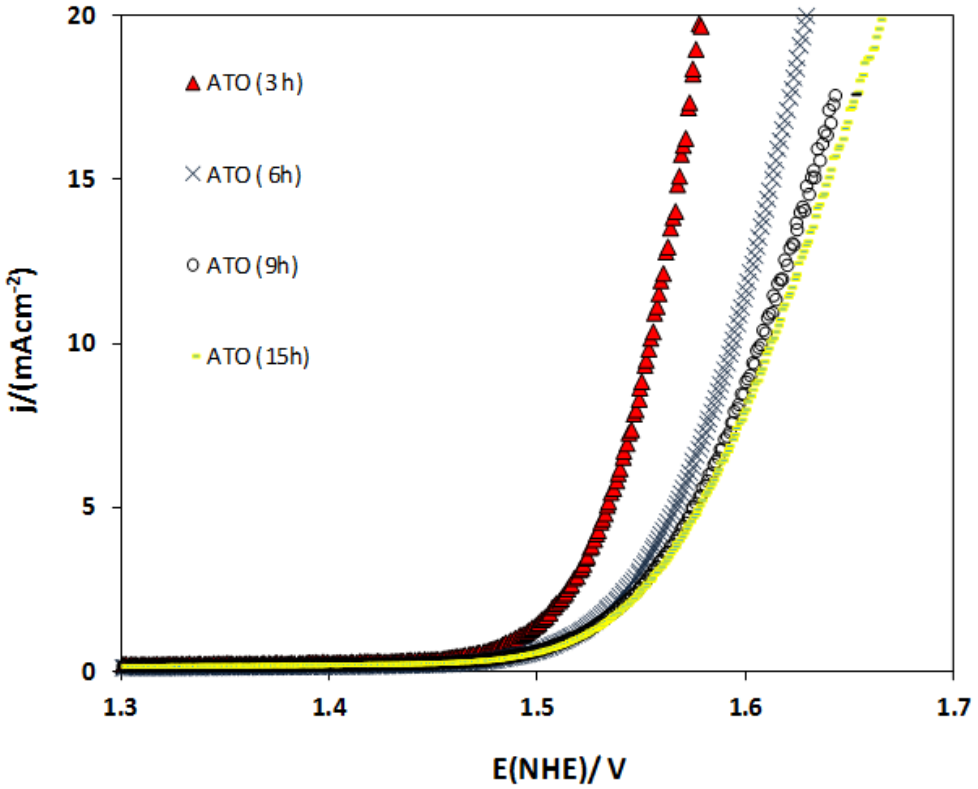

Figure 6. Linear scan voltammograms for OER of IrO_2/ATO (with different heat treatment times) electrodes in N_2 satured 0.5 M H_2SO_4 at ν = 5 mVs^{-1}.

In Figure 7 the linear scan voltammograms for OER with IrO_2 supported on ATO (3h) and IrO_2 supported on carbon are shown [26]. In order to comparison the voltammogram corresponding to OER on Pt/ATO (3h) is included. It can be observed that the oxygen evolution occurs in a potential about 100 mV more negative when the IrO_2 is supported on carbon respect to the onset OER potential obtained with the IrO_2/ATO (3h) electrode. This little difference in overpotential could be put sideways in considering the disadvantage of carbon supports that suffer an easy corrosion at the high potentials used in the electrolysis process. Then the IrO_2 supported on ATO (3h) and finally Pt supported on ATO (3h). In Figure 7 also can be seen the poor catalytic activity of Pt for OER.

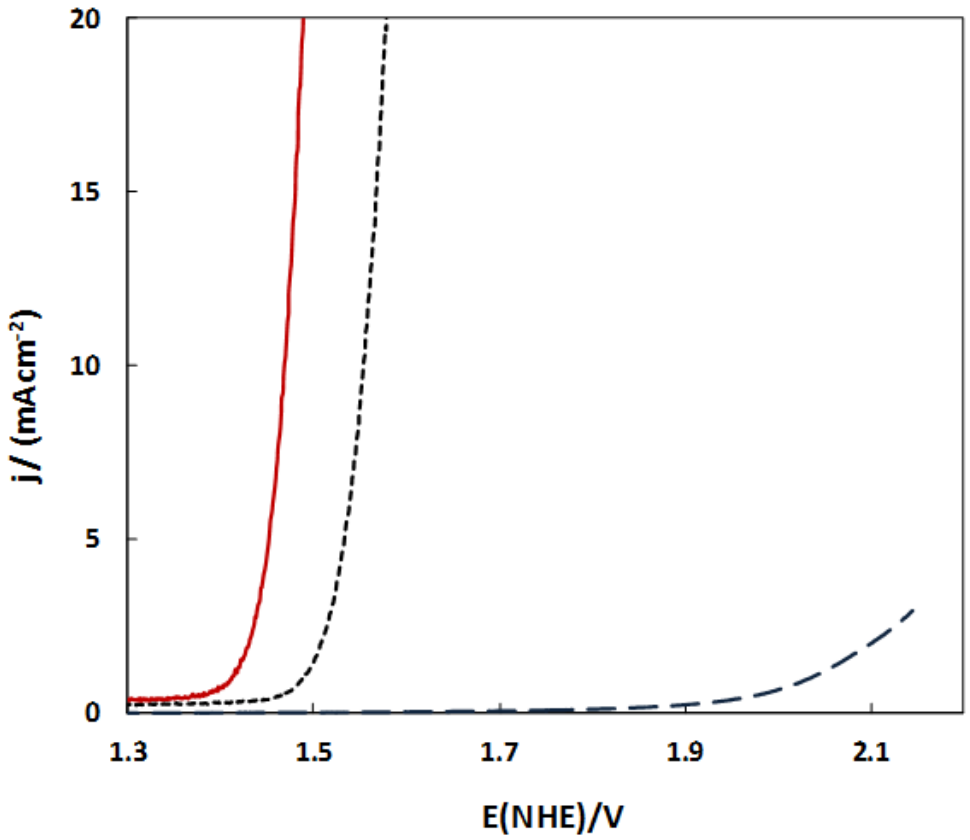

Figure 7. Linear voltammograms for OER on IrO_2/ATO (3h) (blach line), Pt/ ATO (3h) (blue line) and IrO_2/C (red line) electrodes in N_2 satured 0.5 M H_2SO_4, at ν = 5 mVs^{-1}.

Tafel plots were obtained from LSV curves for OER after ohmic drop (IRs) correction due to the electrolyte resistance (Rs). This correction was done by subtracting the IR to the applied potential [27]. The R_s values were obtained by electrochemical impedance spectroscopy (EIS) for each electrode. R_s values were in the 3 Ω – 7.5 Ω interval which are mainly attributed to the solution resistance. Figure 8 shows the Tafel curve for OER on IrO_2 supported on ATO (3h) electrode after IR correction, a Tafel slope (*b*) value of 62 mV dec^{-1} was obtained. A value close to 60 mV dec^{-1} has been observed for OER on some metal oxides in the low overpotential region (η_{low}) [28, 29], for this slope value has been proposed the following mechanism [30]:

$$OH_{ads} \rightarrow O^{-}_{ads} + H^{+} \quad (1)$$

$$O_{ads}^{-} \rightarrow O_{ads} + e \quad (2)$$

$$O_{ads} + O_{ads} \rightarrow O_2 \quad (3)$$

Being the reaction limiting step (rls) for the oxygen evolution process, the reorganization of the oxygen-species over the surface, Ec. (1), before transfer of the first electron. Similarly to the graph shown in Figure 5, Tafel plots were obtained for each of the support under study, showing similar Tafel slope values. These results are presented in Table 2.

Figure 9 shows a comparison of Tafel curves for OER on IrO_2/ATO (3h), IrO_2/ATO (15h) and IrO_2/C electrodes after IR correction. In the potential interval shown, some Tafel curves exhibit two linear slopes related with changes in the EOR kinetic mechanism, in this case the Tafel slope data at high overpotential (η_{high}) show values close to 120 mV dec^{-1}. These results indicate a change in mechanism where the rls is the first transfer electron in the electrolysis of the water molecule. In Figure 9 this behavior is clearly observed for IrO_2/ATO (15h) and IrO_2/C electrodes. The two Tafel slope behavior in OER has been observed in other metal oxide electrodes. The similar values of *b* observed in the IrO_2/ATO and IrO_2/C electrodes, could mean that the OER mechanism is the same in both supports and that the oxygen evolution is developed mainly on the Ir surface.

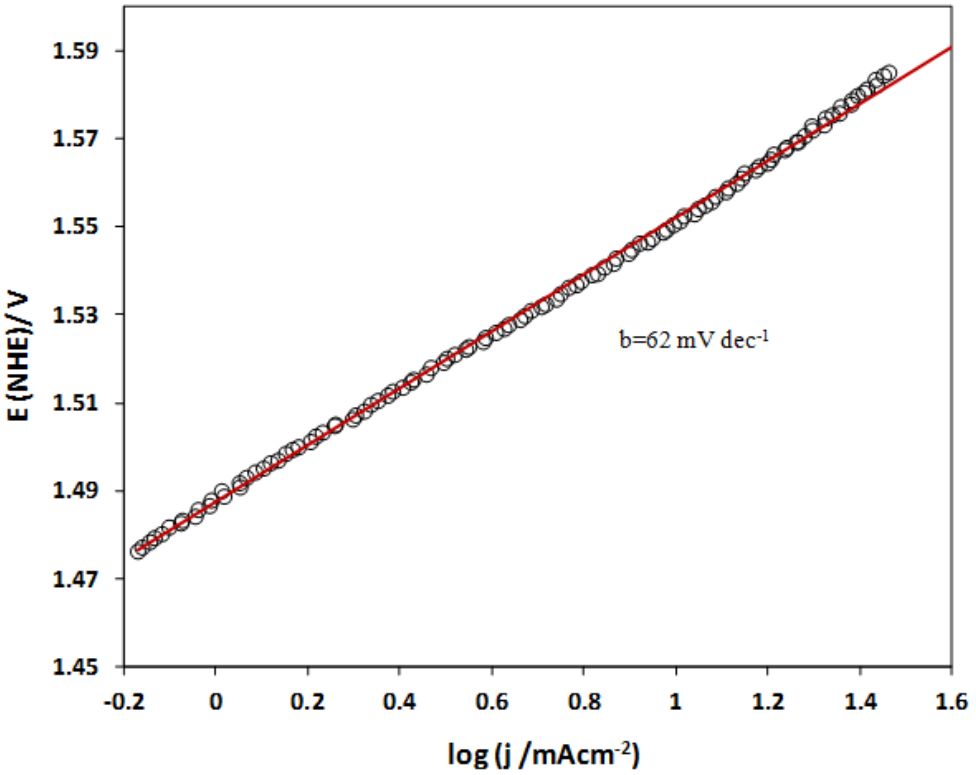

Figure 8. Tafel Plot for OER for IrO_2/ATO (3h) after IR correction.

3.4 Electrochemical impedance spectroscopy performance for OER

EIS measurements for oxygen evolution was carried out on IrO_2/ATO electrodes in O_2 free environment in 0.5 M H_2SO_4 solution, at potensiostatic mode with an anodic potential of 1.57 V.

Figure 10 shows the Nyquist plots for OER on IrO_2 supported on ATO. The depressed semicircles presented in Figure 10 were adjusted by a CNLS fitting to the equivalent circuit presented in Figure 10 [31]:

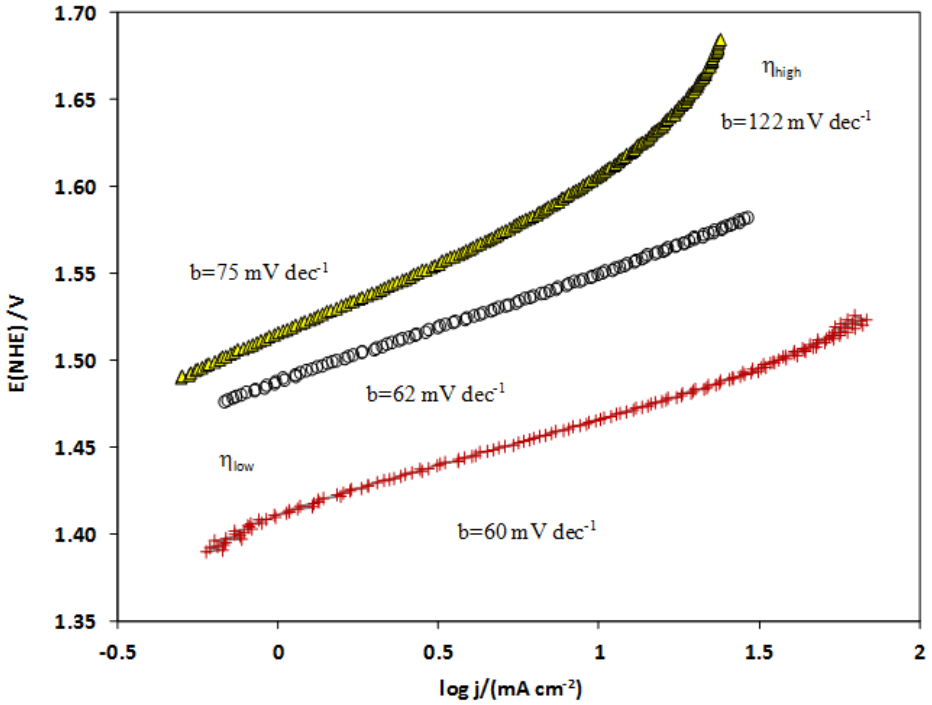

Figure 9. Tafel Plots comparison for OER on IrO_2/ATO (3h) (open circles), IrO_2/ATO (15h) (green triangles) and IrO_2/C (red crosses) after IR correction.

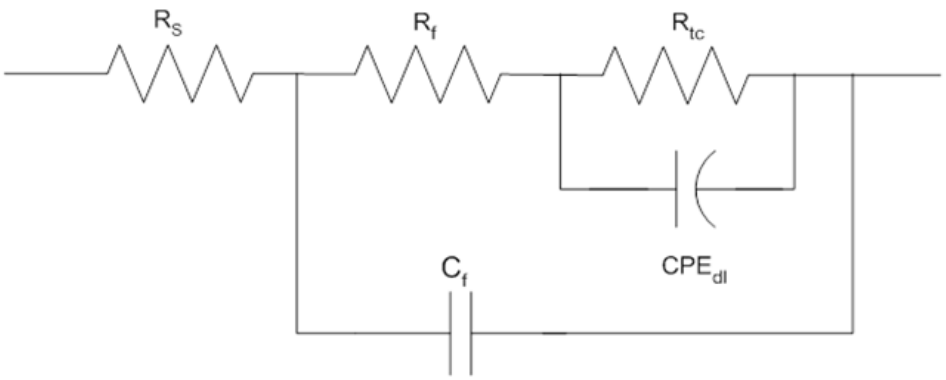

Figure 10. Equivalent circuit used to fit the EIS data for OER on IrO_2/ATO electrodes.

Where R_S is the electrolytic solution resistance, R_f and C_f the resistance and capacitance of the film of catalyst/support/Nafion system, and R_{tc} the resistance of charge transfer associated with the OER in parallel with CPE_{dl} the constant phase element corresponding to the impedance of a double layer over an heterogeneous material electrode surface [31]. The values of R_S and R_{tc} calculated for the IrO_2/ATO electrodes are resumed in Table 2 along with other OER kinetic parameter values.

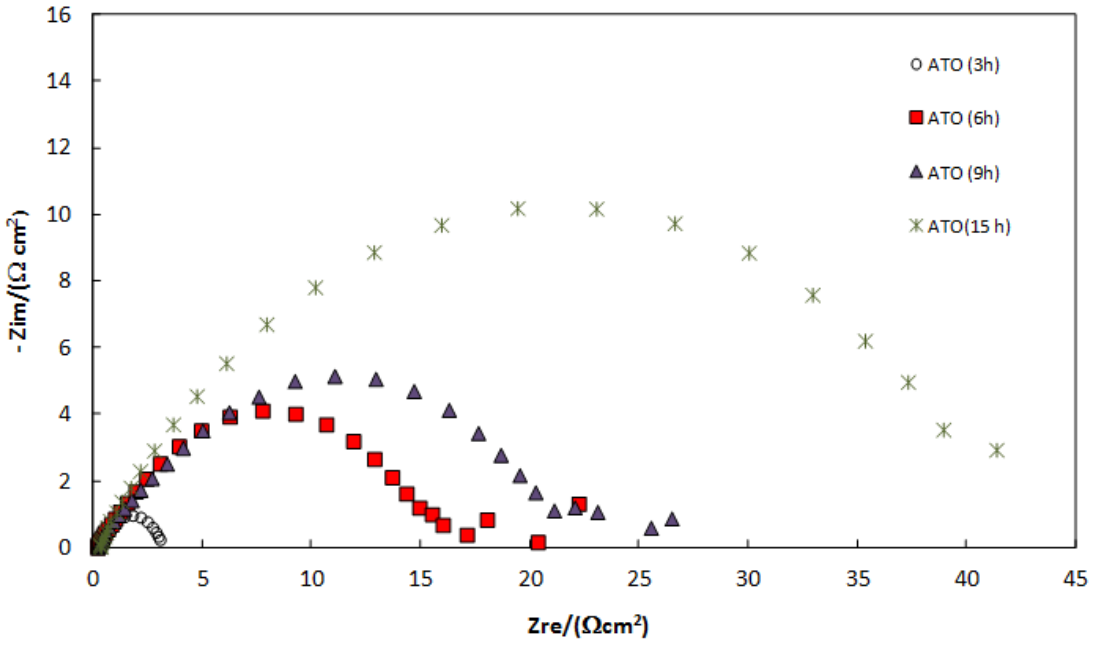

Figure 11. Nyquist plots for OER on IrO_2 /ATO electrodes at anodic potential value of 1.57 V, in O_2-free 0.5 M H_2SO_4 solutions.

In consistency with the LSV results, the Nyquist plots of Figure 11 show that OER is faster when the IrO_2 is supported on ATO (3h), as can be seen by the smaller semicircle in the complex impedance plane. In contrast, the ATO (15h) support shows the bigger Rtc value (c.a. 577 Ω) that means the slowest reaction rate for oxygen evolution on the support materials studied in this work. The rest of ATO supports obtained at other heat treatment times showed intermediate Rtc values.

4. CONCLUSIONS

Electrochemical studies were performed for the OER on IrO_2/ATO electrodes. The OER was evaluated using the ATO obtained with different heat treatment time as support. The results show that the catalytic activity of the electrocatalyst depend on the annealing time of ATO supports, the best behavior corresponding to ATO (3h). In a first sight, are not needed calcination times higher than 3h at 500 °C in order to obtain an adequate ATO support. However further experimentation of ATO is necessary to explore the effect of synthesis thermal times respect to its stability and performance at long times as a catalytic support for the OER.

This study has been shown that the Sb-dopped SnO_2 (ATO) is a promising supports for WE and URFC. The OER onset potential of IrO_2 on ATO is near to observed on the Vulcan carbon, this could mean that the electronic conductivity and catalyst dispersion properties are similar in both support materials, and also the electrokinetic parameters showed that the IrO_2 ATO (3 h) electrode has a similar OER mechanism that IrO_2/C electrode, confirmed by EIS measurements.

ACKNOWLEDGMENTS
The authors wish to thank the mexican CONACyT (Project 167012) for financial support of this work.

References

1. M. Momirlan and T. N. Veziroglu, *Int. J. Hydrogen Energy*, 30 (2005) 795.
2. F. Barbir, *Solar Energy* 78 (2005) 661.
3. A. Marshall, B. Borresen, G. Hagen, M. Tsypkin and R. Tunold, *Energy*, 32 (2007) 431.
4. G. Chen, S. R. Bare and T.E. Mallouk, *J. Electrochem. Soc.* 149 (2002) A1092.
5. S.D. Yim, W.Y. Lee, Y.G. Yoon, Y.J. Sohn, G.G. Park, T.H. Yang and Ch. S. Kim, *Electrochim. Acta*, 50 (2004) 713.
6. S.Song, H.Zhang, X.Ma and Z.Shao, *Int. J. Hydrogen Energy*, 33 (2008) 4955.
7. Y. Zhang, Ch. Wang, N. Wan and Z. Mao, *Int. J. Hydrogen Energy*, 32 (2007) 400.
8. L. H. Franzen, J. E. Vilt, and D. C. Johnson, *J. Electrochem. Soc.*, 4 (1994) 141.
9. E.Gileadi, *Electrode Kinetics for Chemists, Chemical Engineers, and Materials Scientist*, VCH Publishers, John Wiley & Sons, New York (1993).
10. J. Ma, S. Sui and Y. Zhai, *J. Power Sources* , 177 (2008) 470.
11. V. Rashkova, S. Kitova and T. Vitanov, *Electrochim. Acta*, 52 (2007) 3794
12. B. L.García, R.Fuentes and J. W.Weidner, *J.Electrochem. Soc.*, 10 (2007) B108.
13. J. P. Meyers and R. M. Darling, *J. Electrochem. Soc.*, 153 (2006) A1432.
14. M.I.B. Bernardi, C.M. Barrado, L.E.B. Soledade, E.R. Leite, E. Longo and J.A. Varela, *J. Mat. Science*, 13 (2002) 403.
15. J. Santos-Peña, T. Brousse, L. Sánchez, J. Morales and D.M. Schleich, *J. Power Sources*, 97 (2001) 232.
16. V. K. Yatsimirskii, N. P. Maksimovich, A. G. Telegeeva, N. V. Nikitina, and N. A. Boldyreva, *Theoretical and Experimental Chemistry*, 41:3 (2005) 187.
17. R. Subasri and T. Shinohara, *Electrochem. Comm.* 5 (2003) 897.
18. A. T. Marshall and R. G. Haverkamp, *Electrochim. Acta*, 55 (2010) 1978.
19. X. Wu and K. Scott, *Int. J. of Hydrogen Energy*, 36 (2011) 5806.
20. M. Manesse, R. Sanjines, V. Stambouli, R. Boukherrou and S. Szunerits, *Electrochem. Comm,.* 10 (2008) 1041.
21. F. Vicent, E. Morallón, C. Quijada, J. L. Vázquez, A. Aldaz and F. Cases, *J. App. Electrochem.*, 28 (1998) 607.
22. J. C. Cruz , V. Baglio, S. Siracusano, R. Ornelas, L. Ortiz-Frade, L. G. Arriaga, V. Antonucci and A. S. Arico, *J. Nanopart. Res.*, 13 (2011) .
23. J.C. Cruz, *Ph. D. Thesis*, Centro de Investigación y Desarrollo Tecnológico en Electroquímica, México (2012).
24. Y.J. Acosta-Silva, R. Nava, V. Hernández-Morales, S.A. Macías-Sánchez, M.L. Gómez-Herrera and B. Pawelec, *Appl. Catal. B - Envron*. 110 (2011) 108.
25. S. Gilman and D. Chu in *Handbook of fuel cells: Fundamentals, technology and application.* Ed. W. Vielstich, A. Lamm and H. A. Gasteiger, Vol. 2, Ed. John Wiley & Sons, New York (2003).
26. I.L. Escalante-García, S.M. Durón-Torres, J.C. Cruz and Arriaga- Hurtado L.G., Proceedings of the XXIV meeting of the Mexican Society of Electrochemistry, Paper 105, Puerto Vallarta, Jal, México, May 31 – June 5, 2009.
27. J.M. Hu J.Q. Zhang and Ch.N. Cao, *Int. J. Hydrogen Energy*, 29 (2004) 791.
28. J. C. Cruz , V. Baglio, S. Siracusano, V. Antonucci , A. S. Aricò, R. Ornelas, G. Osorio-Monreal, L. Ortiz- Frade, S. M. Durón-Torres and L. G. Arriaga, *Int. J. Electrochem. Science*, 6 (2011) 6607.
29. I.L. Escalante García, S.M. Durón Torres1, J.C. Cruz and L.G. Arriaga Hurtado, *J. New Mat. Electrochem. Systems*, 13, (2010) 227.

30. E. Guerrini and S. Trasatti. *Electrocatalysis in Water Electrolysis in Catalysis for Sustainable Energy Production* (eds. P. Barbaro and C. Bianchini), Wiley-VCH, Weinheim (2009).
31. I. D. Raistrick, D. R. Franceschetti, J. R. Macdonald. The Electrical Analogs of Physical and Chemical Processes in *Impedance Spectroscopy Theory, Experiment and Aplications,* Eds. E. Barsoukov, J.R. Macdonald, JohnWiley & Sons, New Jersey (2005).